Journal of Biomechanics 129 (2021) 110812

Contents lists available at ScienceDirect

Journal of Biomechanics

journal homepage: www.elsevier.com/locate/jbiomech

Finite element modelling of the surgical procedure for placement of a straight electrode array: Mechanical and clinical consequences

B. Areias [a,*], M.P.L. Parente [a,b], F. Gentil [c,d,e], R.M. Natal Jorge [a,b]

[a] INEGI, Institute of Science and Innovation in Mechanical and Industrial Engineering, Porto, Portugal
[b] FEUP, Faculty of Engineering, University of Porto, Porto, Portugal
[c] Escola Superior de Saúde - Politécnico do Porto, Porto, Portugal
[d] Clínica ORL – Dr. Eurico de Almeida, Porto, Portugal
[e] WIDEX, Porto, Portugal

ARTICLE INFO

Keywords:
Cochlea
Cochlear implant
Intra-cochlear damage
Straight electrode
Finite element method

ABSTRACT

A cochlear implant is an electronic device implanted into the cochlea to directly stimulate the auditory nerve. Such device is used in patients with severe-to-profound hearing loss. The cochlear implant surgery is safe, but involves some risks, such as infections, device malfunction or damage of the facial nerve and it can result on a poor hearing outcome, due to the destruction of any present residual hearing. Future improvements in cochlear implant surgery will necessarily involve the decrease of the intra-cochlear damage. Several implant related variables, such as materials, geometrical design, processor and surgical techniques can be optimized in order for the patients to partially recover their hearing capacities The straight electrode is a type of cochlear implant that many authors indicate as being the less traumatic.

From the finite element analysis conducted in this work, the influence of the insertion speed, the friction coefficient between the cochlear wall and the electrode array, and several configurations of the cochlear implant tip were studied. The numerical simulations of the implantation showed the same pattern of the insertion force against insertion depth, thus indicating the different phases of the insertion. Results demonstrated that lower insertion speeds, friction coefficients and tip stiffness, led to a reduction on the contact pressures and insertion force. It is expected that these improved configurations will allow to preserve the residual hearing while reducing surgical complications.

1. Introduction

Hearing and balance are the crucial functions of the inner ear which allow the perception and discrimination of sounds and accelerations. The cochlea and the semicircular canals, which form the inner ear, are located within the petrous part of the temporal bone, being positioned according to Fig. 1a. There are many environmental factors that can damage the hair cells within the inner ear, thus causing hearing loss (Kountakis, 2013; Eshraghi et al., 2012; Korver et al., 2017). Currently, congenital hearing loss affects between 1–3 per 1000 live births, according to Allen and Goldman (2020).

Cochlear implant surgery is an effective treatment indicated for deafness and severe hearing loss. A cochlear implant (Fig. 1b) consists in an external part and an internal part. As refereed by Kha and Chen (2012) and Stover and Lenarz (2009), the electrode array (internal part) is usually made with platinum wires, allowing for a good resistance to corrosion, embedded in a silicon elastomer, which provide a good malleability during the insertion process.

Cochlear implants are divided in perimodiolar and straight. Each cochlear implant type has its advantages and disadvantages, and each of them is better suitable for a certain type of pathology and condition of the cochlea. As mentioned by Gibson and Boyd (2016), the slim straight electrode implant demonstrates useful preservation of residual hearing. On the other hand, in the work of Eshraghi et al. (2003), the straight electrodes may present an equal or even a greater risk of damage when compared with the perimodiolar implant. Thus, depending of the perspective (damage, preservation, risk), different conclusions can be obtained. Such discrepancies can be explained by the experience of the surgeon and by the surgical techniques utilized. Overall, damage is expected in the lateral wall due to the insertion of the straight electrode (Risi, 2018). The insertion of a cochlear implant

* Correspondence to: INEGI, Institute of Science and Innovation in Mechanical and Industrial Engineering, Rua Dr. Roberto Frias 400, Porto 4200-465, Portugal.
E-mail addresses: bareias@fe.up.pt (B. Areias), mparente@fe.up.pt (M.P.L. Parente), fernanda.fgnanda@gmail.com (F. Gentil), rnatal@fe.up.pt (R.M. Natal Jorge).

https://doi.org/10.1016/j.jbiomech.2021.110812
Accepted 7 October 2021
Available online 16 October 2021

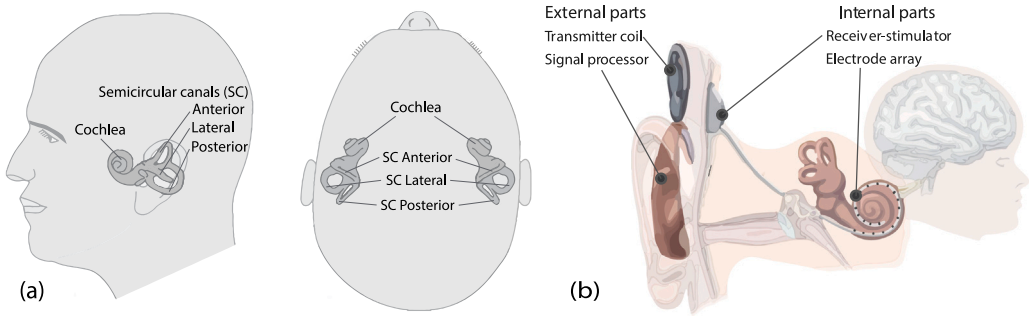

Fig. 1. (a) Position and orientation of the inner ear, (b) Illustration of the cochlear implant position with external and internal part, adapted from Kral (2013).

is performed through the scala tympani, and there are currently three surgical approaches in use: the cochleostomy technique, the round window technique and the enlarged round window technique (Khater and El-Anwar, 2017; Richard et al., 2012).

Several works in the literature, report that higher insertion speeds cause significant increase of the insertion forces (Kontorinis et al., 2011; Rajan et al., 2013; Aebischer et al., 2021). However, the contact pressure between the cochlear wall and the electrode array is not easy to experimentally measure, and numerical models should be developed in order to increase the knowledge of the complications related with the cochlear implant surgery. In relation to the friction, its increasing generally increases the insertion forces as shown by Goury et al. (2016). Also, the study of Dohr et al. (2021) reveals a non-linear increase in electrode array friction, when insertion speed raises, thus showing a relationship between the insertion speed and the friction.

Current research is focused on new strategies relating to the electrode design, in order to improve the neuronal health (by developing less traumatic electrodes) and the spatial selectivity. The finite element method is known as a tool which can help the medical community in the search of new surgical techniques and consequently to improve old procedures. The present study uses the finite element method in order to evaluate and obtain new ways of reducing the intra-cochlear trauma, based on the study of several parameters related with the cochlear implant insertion, such as insertion speed, friction coefficient and implant stiffness.

2. Materials and methods

The anatomical geometry of the human cochlea was obtained from a magnetic resonance imaging scan, of a male patient, without cochlear pathologies. The Mimics software (v19.0.0.347, Materialise) was then used to perform a manual segmentation of the cochlear wall. A straight electrode (Fig. 2) was considered in order to simulate the insertion of the cochlear implant. The SolidWorks software 2020 was used for modelling the straight electrode, which had a length of 25 mm and a diameter ranging between 0.55 mm at proximal end and 0.3 mm at distal end. The distal side ended a hemispherical tip. Dimensions and shape of the electrode array were based on the standard commercially available CI622 cochlear implant manufactured by the Cochlear medical device company (Cochlear Limited, 2019). The round window membrane approach was applied. This approach is the less aggressive since only the round window membrane is extracted. Although it can lead to more risks and insertion trauma as mentioned by Zhou et al. (2015). However, this work applied the round window membrane approach, since it should be the approach used, when the anatomy is favourable, as mentioned by Richard et al. (2012).

The finite element model includes the cochlear wall and the electrode array of the straight cochlear implant. To conduct the numerical analysis, the electrode array was meshed with linear hexahedral elements, with reduction integration (C3D8R). The cochlear wall was modelled with 4-node shell elements (S4). In total, the finite element mesh for the electrode array was composed by 9036 nodes. The cochlear wall was discretized with 28137 nodes. All numerical analyses were carried out using the finite element Abaqus/Explicit software package (Dassault Systemes, 2016). A mesh convergence study was conducted before all simulations for ensuring the accuracy of the finite element analysis. An explicit dynamics procedure using an explicit central-difference time integration rule was applied. The accelerations at the beginning of an increment are computed using Eq. (1).

$$\ddot{u}^N_{(i)} = \left(M^{NJ}\right)^{-1}\left(P^J_{(i)} - I^J_{(i)}\right) \tag{1}$$

where $\ddot{u}^N_{(i)}$ is the acceleration at the increment i, M^{NJ} is the mass matrix, $P^J_{(i)}$ is the applied load vector, and $I^J_{(i)}$ is the internal force vector.

The central-difference integration operator is explicit, thus the kinematic states $\left(\dot{u}^N_{\left(i+\frac{1}{2}\right)}\right.$ and $\left.u^N_{(i+1)}\right)$ are calculated using the known values from the previous increment $\left(\dot{u}^N_{\left(i-\frac{1}{2}\right)}\right.$ and $\left.\ddot{u}^N_{(i)}\right)$, according to Eqs. (2) and (3).

$$\dot{u}^N_{\left(i+\frac{1}{2}\right)} = \dot{u}^N_{\left(i-\frac{1}{2}\right)} + \frac{\Delta t_{(i+1)} + \Delta t_{(i)}}{2}\ddot{u}^N_{(i)} \tag{2}$$

$$u^N_{(i+1)} = u^N_{(i)} + \Delta t_{(i+1)}\dot{u}^N_{\left(i+\frac{1}{2}\right)} \tag{3}$$

The explicit procedure requires no iterations and no tangent stiffness matrix, the scheme is conditionally stable and thus smaller time steps are required. In Abaqus, the size of the stable time increment can be computed using Eq. (4).

$$\Delta t \approx \frac{L_{min}}{c_d} \tag{4}$$

where L_{min} is the smallest element dimension in the entire model and c_d is the dilatational wave speed.

In order to establish the friction between two surfaces in contact, Abaqus uses the Coulomb friction model. These surfaces can carry shear stresses up to a certain magnitude across their interface before starting to slide. The critical shear stress is defined in the Coulomb friction model as τ_{crit}, and depends of the normal contact pressure, p according to the following Equation: $\tau_{crit} = \mu p$.

In the present study different implant insertion speeds ($v_{insertion}$: 0.25, 0.5, 1 and 2 mm s^{-1}) and different friction coefficients (μ: 0, 0.05, 0.1, 0.2, 0.3) between the cochlear lateral wall and the cochlear implant were simulated. The insertion speed values used on this work are in accordance with other studies available on the literature, which refer to speeds ranging between 0.25 mm s^{-1} (Rajan et al., 2013; Todt et al., 2014) to 1.6 mm s^{-1} (Kontorinis et al., 2011). The friction values were based on the experimental work of Kha and Chen (2006), in addition a possible critical case of 0.3 was carried out. The cochlear wall was considered with elastic properties, E=14 100 MPa, ν=0.3 and a density of ρ=2000 kg m^{-3} (Areias et al., 2016; Sun et al., 2002; Gentil et al., 2011). The Young's modulus, Poisson's ratio and density assumed for the cochlear implant were E=1000 MPa, ν=0.3 and a density of ρ=1000 kg m^{-3} (Chen et al., 2003; Kha and Chen, 2012). As result, the

Table 1
Mechanical properties used, for different tip lengths.

Tip length [mm]	E [MPa]	ν [-]	ρ [kg m^{-3}]
2.5	250 (25 %) 500 (50 %) 50 (75 %)	0.3	1000
5	250 (25 %) 500 (50 %) 750 (75 %)		

mean contact pressure at the cochlear implant tip and the insertion force was obtained. The mean contact pressure at the tip is given by the average of the contact pressure between the cochlear implant tip and the cochlear wall. For this average, only the pressure values from the superficial nodes at the hemispherical tip were considered.

In order to study the influence of the tip length and stiffness, different tip lengths (Fig. 2) and Young's modulus were considered. The tip length and the Young's modulus parameters were assumed. In relation to the tip length, the dimensions of 2.5 mm and 5 mm represents 10% and 20% of the electrode array length. Such assumptions will allow to evaluate the influence of the electrode array tip stiffness during the insertion procedure. The values are summarized in Table 1.

In all numerical simulations, the petrous part of the temporal bone was fixed in all degree of freedom and an imposed displacement of 25 mm was applied at the proximal surface of the cochlear implant, thus leading to a complete insertion of the electrode array.

3. Results

In order to understand how the angular position of the implant tip evolves during the insertion procedure, a first study was conducted, using an insertion speed of 1 mm s^{-1} and considering no friction. Fig. 3 shows the relation between the insertion depth in millimetres and the angular position of the implant tip, during the insertion. Since this is mainly a geometrical constrained problem, no other velocities were considered for this first study. A linear regression was also carried out, which allows to observe that the curve follows approximately a linear regression except between the 10 mm and 18 mm deep, where a certain deviation was verified. The initial contact was reached at about 8 mm deep. After that, an adaptation of the electrode array to the cochlear wall was verified.

Franz and Clark (1987) indicated the range between the 8 mm and 10 mm of insertion as the most critical range of the insertion process. Similarly, De Seta et al. (2017) mentioned the critical range between 150° and 180°. There appears to be a connection between the achieved deviation, due to the electrode adaptation, and the damage induced by the cochlear implant.

Since the insertion speed is a variable of the insertion procedure, different insertion speeds were simulated and its influence on the contact pressures computed. Fig. 4 shows the evolution between the mean contact pressure at the cochlear implant tip and the insertion depth, for different insertion speeds. No differences in contact pressures were found for insertions with speeds lower than 1 mm s^{-1}. For 2 mm s^{-1} insertion speed, an increase in the contact pressure was verified, after an insertion length of 15 mm. This difference amounted to approximately 50 %, for an insertion length of 25 mm.

Fig. 5 shows the relation between the insertion force and the insertion depth. All numerical curves follow the same trend, among the different insertion speeds. The initial contact occurs for an insertion depth of 8 mm. After the initial contact, a sharp increase in the insertion force was identified, thus showing the adaptation of the electrode array to the cochlear wall. A second sharp increase in the insertion force was found, for all insertion speeds, after a insertion length of 20 mm. In the final stage of the electrode array insertion, the insertion force increases approximately 250 % in relation to the 20 mm insertion length.

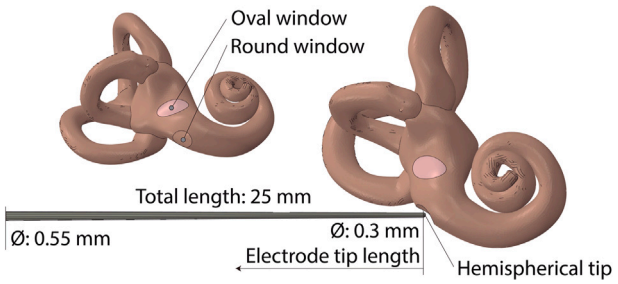

Fig. 2. Finite element model of the CI622 cochlear implant and the cochlear wall. Demonstration of the electrode tip length.

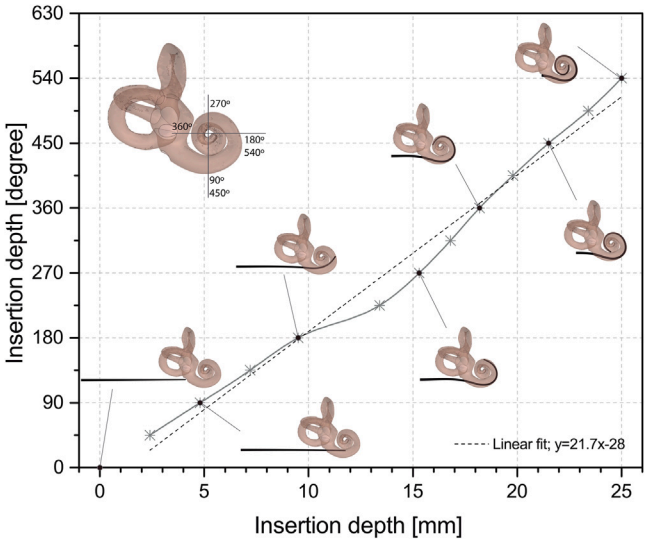

Fig. 3. Relation between the insertion depth in millimetres vs in degrees ($v_{insertion}$=1 mm s^{-1}, without friction).

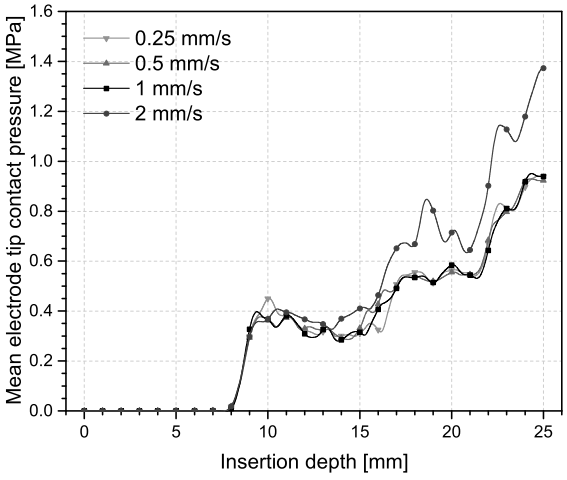

Fig. 4. Mean electrode tip contact pressure during the insertion of 25 mm, for different insertion speeds (0.25, 0.5, 1 and 2 mm s^{-1}).

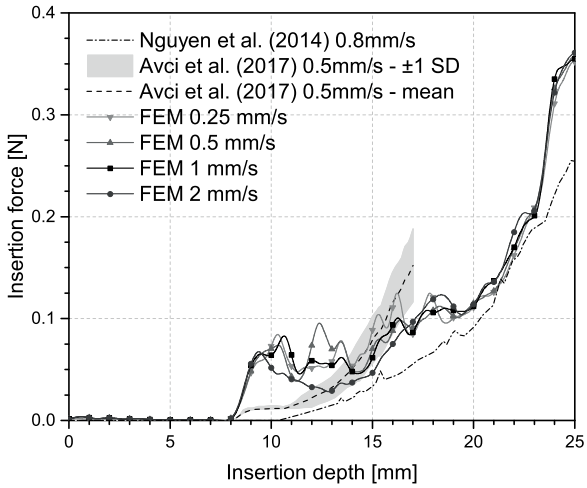

Fig. 5. Insertion force during the insertion of 25 mm, for different insertion speeds (0.25, 0.5, 1 and 2 mm s^{-1}). Experimental data reported from Nguyen et al. (2014) and Avci et al. (2017) included in order to validate the model. The grey area indicates ±1 SD of the Avci et al. (2017).

In order to validate the model, two experimental data reported in the literature were also included in the Fig. 5. The study conducted by Nguyen et al. (2014) comprise the insertion of eight electrode arrays with an in-house made motorized insertion tool using an actuator speed controlled via a laboratory set at 0.8 mm s^{-1}. Another experimental study carried out by Avci et al. (2017) at a speed of 0.5 mm s^{-1} was also represented.

The differences observed between the 8 mm and 12 mm, can be justified by the use of a different angle of insertion. The tangent insertion of the electrode array in relation to the lateral wall allows a decrease in the initial peak force, however this type of procedure usually require the drilling of the round window or a cochleostomy. Torres et al. (2018) used a robot-based insertion coupled to a navigation system to assess the relationship between the insertion axis and intracochlear trauma. The authors mentioned that a higher angle of approach to the scala tympani centreline leads to an early contact of the array tip with the walls of the cochlea. This phenomenon may cause an osseous spiral lamina fracture in the first 90 degrees, a proximal array translocation and the probability of cross the basilar membrane several times. Our study considered the extraction of the round window, thus the insertion angle was not perfectly tangent to the cochlear walls, thus causing the sharp increase of the insertion force.

Among the different speeds tested, no major differences in the insertion force were found. In the study of Kontorinis et al. (2011) a proportional correlation of the cochlear implant insertion speed with the insertion force was obtained. In contrast, Rau et al. (2010), showed higher values of insertion force when implants were inserted with lower speeds. Some controversy exists in the literature, therefore the speeds usually used are very small to involve inertial effects.

The matrix presented in Fig. 6 shows the influence of the friction coefficient on the von Mises stress distribution in the cochlear implant, for different insertion depths and for an insertion speed of 1 mm s^{-1}. The friction coefficients were based on the experimental data of Kha and Chen (2006), which published values between 0.12 and 0.19 in conditions without lubricants and between 0.04 and 0.15 in conditions with glycerin and sorbelene. No major influence of the friction coefficient was verified on the von Mises stress distribution, along the cochlear implant. The higher differences appears for an insertion depth of 25 mm and for the higher friction coefficient used ($\mu = 0.3$), where the cochlear implant started to buckle, near the round window. A decrease in the angular position of the cochlear implant, during insertion is also notorious as the friction coefficient increases. Outside the cochlear partition, on the cochlear implant an increase in the curvature as the friction increased is evident, thus showing the increasing resistance during the insertion derived from the increasing friction coefficient (Fig. 6, red arrows in the second row).

Frictional conditions are crucial in the evaluation of the contact stresses. As mentioned by Kha and Chen (2006) small changes in the frictional coefficients can lead to large differences in the contact stresses. Fig. 7 shows the relation between the mean contact pressure at the cochlear implant tip and the insertion depth, for different friction coefficients. An insertion speed of 1 mm s^{-1} was considered for all curves. As expected, the lowest mean contact pressure was obtained for the frictionless case. For the cases with friction, there is no notorious differences between an insertion depth of 5 mm (90°) and 15 mm (270°). However, a decrease of approximately 40 % was obtained between the frictionless case and all cases with friction. After 15 mm deep, the mean contact pressure increases with friction, except for the case $\mu = 0.3$. In this case ($\mu = 0.3$), the presence of the second peak (15 mm - 20 mm) was not evident. Such discrepancy can be related with the delay on the insertion of the cochlear implant due the friction between the electrode array and the endosteum lining, and also by the initiation of buckling which is visible in this case (Fig. 6), which reduces the pressure on the tip. At the end of the cochlear implant insertion, the buckling of the electrode array causes an abrupt decrease of the mean contact pressure, for the higher friction coefficient.

Fig. 8 shows the influence of the friction coefficient on the insertion force, for an insertion speed of 1 mm s^{-1}. The insertion force increase with increasing friction coefficients. Comparing with the frictionless case, there was an increase of the maximum insertion force in the order of 1.22 times with $\mu = 0.05$, of 1.67 times with $\mu = 0.1$, of 3.8 times with $\mu = 0.2$ and of 9.4 times with $\mu = 0.3$. Therefore, an exponential increase of the maximum insertion force was obtained. Similarly, in Fig. 7, the fast decrease of the insertion force for the higher friction coefficient ($\mu = 0.3$) is a consequence of the electrode array buckling. Hence, for high friction coefficients ($\mu > 0.2$), the buckling of electrode array may occur, thus damaging the cochlea near the round window.

Fig. 9a shows the mean contact pressure at the implant tip for different tip configurations. Overall, there was a decrease of the mean contact pressure as the Young's modulus of the tip decreased. No differences of the insertion trajectory were identified between all cases. The case with a Young's modulus of 250 MPa and a tip length of 5 mm showed an almost linear increase of the mean contact pressure, which can be correlated with fewer damages on the cochlear wall due to the smooth and progressive insertion. As mentioned by Dhanasingh and Jolly (2017), the damage of the cochlear wall can lead to the formation of new bone growth which could compromise the residual cochlear function. The case with a Young's modulus of 250 MPa and a tip length of 2.5 mm resulted in the lowest contact pressure with a reduction of 75 % when compared with the homogeneous case. The insertion force for the different tip configurations is shown in Fig. 9b. No major differences were detected between all cases. Overall, a decrease in the maximum insertion force was obtained in all cases with modified tip when compared with the homogeneous implant case.

4. Conclusions

Cochlear implant electrode insertion force and contact pressure between the implant tip and the cochlear wall can influence the intracochlear damage and the preservation of the residual hearing. A series of steps takes place during the cochlear implant insertion. Such stages were investigated in this numerical study. The relation between the insertion depth and the angular position of the implant tip follows approximately a linear regression. For an insertion depth between 10 mm and 18 mm the initial contact was established and a consequent adaptation of the cochlear implant to the cochlear wall occurred.

The study involving different insertion speeds showed that lower speeds result in lower contact pressures at the implant tip. In relation

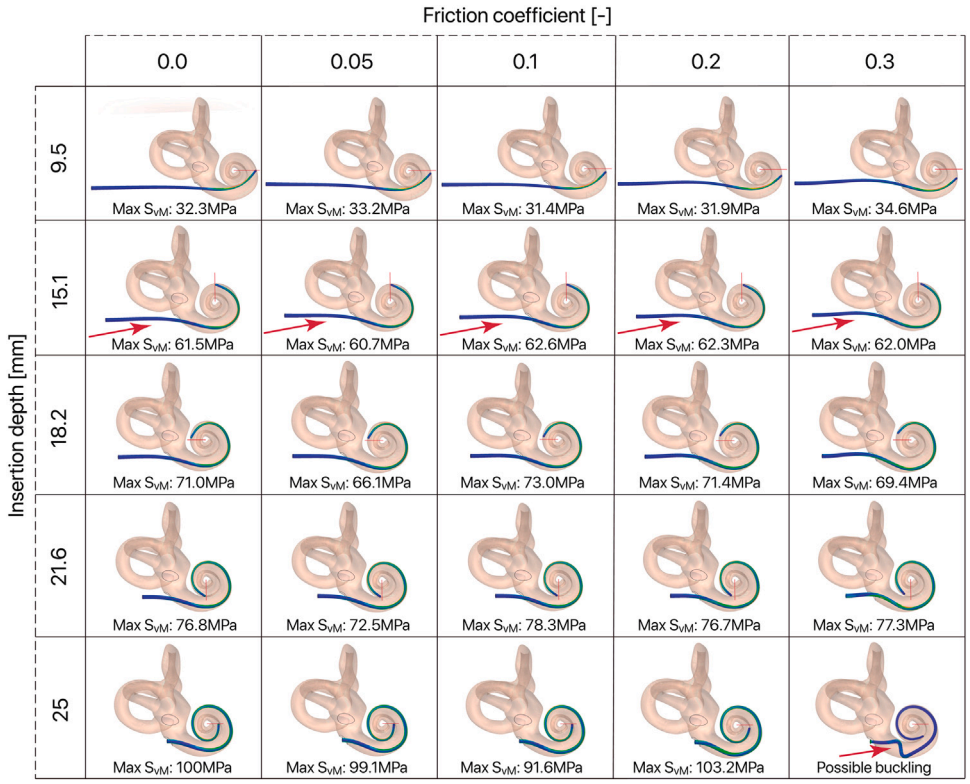

Fig. 6. Influence of the friction coefficient between the cochlear implant and the scala tympani walls on the maximum von Mises stress (S_{vM}) present on the cochlear implant, for different insertion depths.

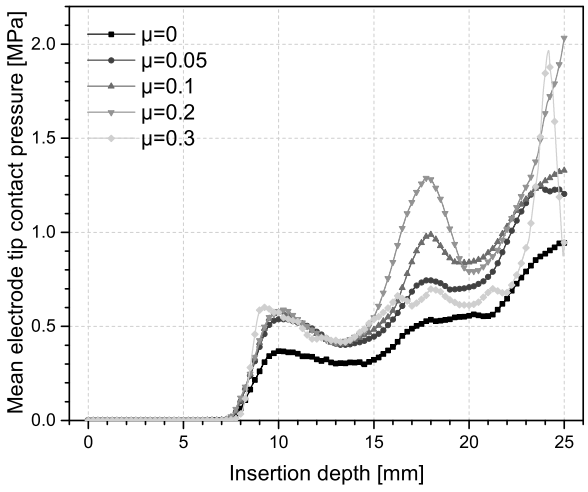

Fig. 7. Mean electrode tip contact pressure during the insertion of 25 mm, for different friction coefficients (0, 0.05, 0.1, 0.2 and 0.3).

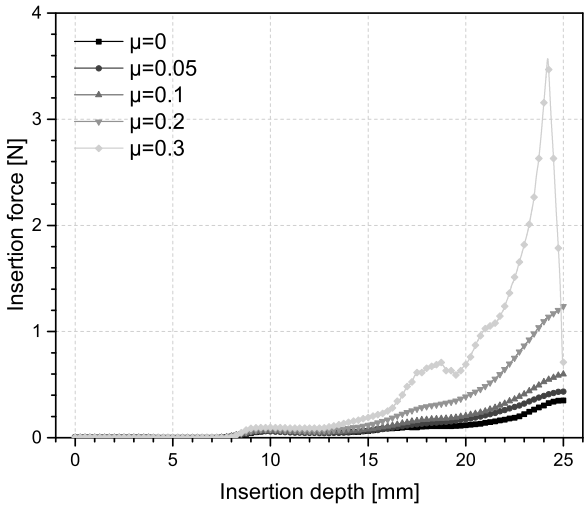

Fig. 8. Insertion force during the insertion of 25 mm, for different friction coefficients (0, 0.05, 0.1, 0.2 and 0.3).

to the friction coefficient, there was an abrupt decrease of the mean contact pressure and insertion force in the case of $\mu = 0.3$, thus showing a buckling of the electrode array. The friction coefficient exhibit no influence on the von Mises stresses along the electrode array. However, an increase in the insertion force as the friction coefficient increased was achieved. With respect to the study of the cochlear implant tip properties, a decrease in the mean contact pressure was obtained as the Young's modulus decreased. No differences in the electrode array trajectory were identified between all the studied cases. The homogeneous implant exhibited the highest insertion force compared with the modified tip cases.

In order to reduce the lateral displacement of the electrode array, outside the cochlear duct (probability of buckling) and increase the cochlear implant stability, a stiffer electrode array at the basal portion should be developed. The results showed that a soft tip can decrease the contact pressure, thus resulting in a less damage of the cochlear walls. It is therefore necessary to numerically study novel cochlear implants with gradual stiffness in order to avoid high contact pressures with the cochlear walls and the basilar membrane, which can lead to its perforation and consequently, the loss of the endo-cochlear potential and the loss of the residual hearing.

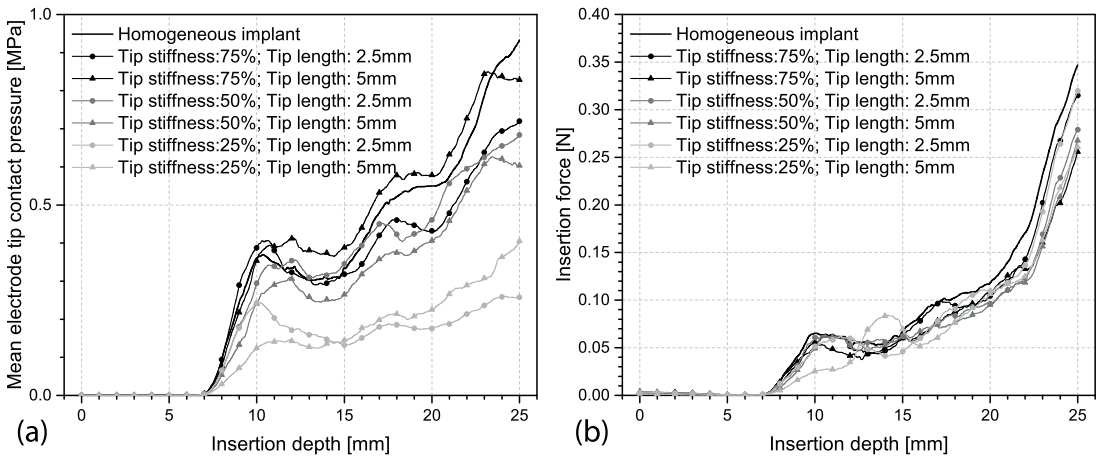

Fig. 9. (a) Mean electrode tip contact pressure during the electrode insertion, for different tip mechanical properties (Table 1), (b) Insertion force during the electrode insertion, for different tip mechanical properties (Table 1).

Declaration of competing interest

The authors declare that they have no known competing financial interests or personal relationships that could have appeared to influence the work reported in this paper.

Acknowledgements

The authors truly acknowledge the funding provided by Ministério da Ciência, Tecnologia e Ensino Superior - Fundação para a Ciência e a Tecnologia (Portugal), under grant: SFRH/BD/129397/2017. This research was also supported by the Portuguese Foundation of Science and Technology under the research project UIDB/50022/2020.

References

Aebischer, P., Mantokoudis, G., Weder, S., Anschuetz, L., Caversaccio, M., Wimmer, W., 2021. In-vitro study of speed and alignment angle in cochlear implant electrode array insertions. IEEE Trans. Biomed. Eng.

Allen, S.B., Goldman, J., 2020. Syndromic sensorineural hearing loss. In: StatPearls [Internet]. StatPearls Publishing, Treasure Island (FL).

Areias, B., Santos, C., Natal Jorge, R.M., Gentil, F., Parente, M.P.L., 2016. Finite element modelling of sound transmission from outer to inner ear. Proc. Inst. Mech. Eng. H 230, 999–1007.

Avci, E., Nauwelaers, T., Hamacher, V., Kral, A., 2017. Three-dimensional force profile during cochlear implantation depends on individual geometry and insertion trauma. Ear Hear 38 (3), 168–179.

Chen, B.K., Clark, G.M., Jones, R., 2003. Evaluation of trajectories and contact pressures for the straight nucleus cochlear implant electrode array - a two-dimensional application of finite element analysis. Med. Eng. Phys. 25 (2), 141–147.

Cochlear Limited, 2019. Cochlear limited. Available at https://www.cochlear.com. (Accessed 10 February 2020).

Dassault Systemes, 2016. ABAQUS Analysis User's Guide.

De Seta, D., Torres, R., Russo, F.Y., Ferrary, E., Kazmitcheff, G., Heymann, D., Amiaud, J., Sterkers, O., Bernardeschi, D., Nguyen, Y., 2017. Damage to inner ear structure during cochlear implantation: Correlation between insertion force and radio-histological findings in temporal bone specimens. Hear. Res. 344, 90–97.

Dhanasingh, A., Jolly, C., 2017. An overview of cochlear implant electrode array designs. Hear. Res. 356, 93–103.

Dohr, D., Fiedler, N., Schmidt, W., Grabow, N., Mlynski, R., Schraven, S.P., 2021. Frictional behavior of cochlear electrode array is dictated by insertion speed and impacts insertion force. Appl. Sci. 11 (11), 5162.

Eshraghi, A.A., Nazarian, R., Telischi, F.F., Rajguru, S.M., Truy, E., Gupta, C., 2012. The cochlear implant: historical aspects and future prospects. Anat. Rec. (Hoboken) 295 (11), 1967–1980.

Eshraghi, A.A., Yang, N.W., Balkany, T.J., 2003. Comparative study of cochlear damage with three perimodiolar electrode designs. Laryngoscope 113 (3), 415–419.

Franz, B.K.H.G., Clark, G.M., 1987. Refined surgical technique for insertion of banded electrode array. Ann. Otol. Rhinol. Laryngol. 96 (1), 15–17.

Gentil, F., Parente, M., Martins, P., Garbe, C., Jorge, R.N., Ferreira, A., Tavares, J.M.R.S., 2011. The influence of the mechanical behaviour of the middle ear ligaments: a finite element analysis.. Proc. Inst. Mech. Eng. H 225, 68–76.

Gibson, P., Boyd, P., 2016. Optimal electrode design: Straight versus perimodiolar. Eur. Ann. Otorhinolaryngol.-Head Neck Dis. 133, S63–S65.

Goury, O., Nguyen, Y., Torres, R., Dequidt, J., Duriez, C., 2016. Numerical simulation of cochlear-implant surgery: Towards patient-specific planning. In: 19th International Conference on Medical Image Computing & Computer Assisted Intervention. MICCAI 2016. vol. 9900, pp. 500–507.

Kha, H., Chen, B., 2006. Determination of frictional conditions between electrode array and endosteum lining for use in cochlear implant models. J. Biomech. 39 (9), 1752–1756.

Kha, H., Chen, B., 2012. Finite element analysis of damage by cochlear implant electrode array's proximal section to the basilar membrane. Otol. Neurotol. 33 (7), 1176–1180.

Khater, A., El-Anwar, M.W., 2017. Methods of hearing preservation during cochlear implantation. Int. Arch. Otorhinolaryngol. 21, 297–301.

Kontorinis, G., Lenarz, T., Stover, T., Paasche, G., 2011. Impact of the insertion speed of cochlear implant electrodes on the insertion forces. Otol. Neurotol. 32 (4), 565–570.

Korver, A., Smith, R., Camp, G., Schleiss, M., Bitner-Glindzicz, M., Lustig, L., Usami, S.-i., Boudewyns, A., 2017. Congenital hearing loss. Nat. Rev. Dis. Primers 3, 16094.

Kountakis, S.E., 2013. Encyclopedia of Otolaryngology, Head and Neck Surgery. Springer Reference, Heidelberg, New York, p. 5 volumes.

Kral, A., 2013. Auditory critical periods: A review from system's perspective. Neuroscience 247, 117–133.

Nguyen, Y., Kazmitcheff, G., De Seta, D., Miroir, M., Ferrary, E., Sterkers, O., 2014. Definition of metrics to evaluate cochlear array insertion forces performed with forceps, insertion tool, or motorized tool in temporal bone specimens. Biomed. Res. Int. 2014, 532570.

Rajan, G.P., Kontorinis, G., Kuthubutheen, J., 2013. The effects of insertion speed on inner ear function during cochlear implantation: a comparison study. Audiol. Neurootol. 18 (1), 17–22.

Rau, T.S., Hussong, A., Leinung, M., Lenarz, T., Majdani, O., 2010. Automated insertion of preformed cochlear implant electrodes: evaluation of curling behaviour and insertion forces on an artificial cochlear model. Int. J. Comput. Assist. Radiol. Surg. 5 (2), 173–181.

Richard, C., Fayad, J.N., Doherty, J., Linthicum, J., 2012. Round window versus cochleostomy technique in cochlear implantation: histologic findings. Otol. Neurotol. 33 (7), 1181–1187.

Risi, F., 2018. Considerations and rationale for cochlear implant electrode design - past, present and future. J. Int. Adv. Otol. 14 (3), 382–391.

Stover, T., Lenarz, T., 2009. Biomaterials in cochlear implants. GMS Curr. Top. Otorhinolaryngol. Head Neck Surg. 8, Doc10.

Sun, Q., Gan, R.Z., Chang, K.-H., Dormer, K.J., 2002. Computer-integrated finite element modeling of human middle ear. Biomech. Model. Mechanobiol. 1, 109–122.

Todt, I., Mittmann, P., Ernst, A., 2014. Intracochlear fluid pressure changes related to the insertional speed of a CI electrode. Biomed. Res. Int.

Torres, R., Drouillard, M., De Seta, D., Bensimon, J.L., Ferrary, E., Sterkers, O., Bernardeschi, D., Nguyen, Y., 2018. Cochlear implant insertion axis into the basal turn: A critical factor in electrode array translocation. Otol. Neurotol. 39 (2), 168–176.

Zhou, L., Friedmann, D.R., Treaba, C., Peng, R., Roland, Jr., J.T., 2015. Does cochleostomy location influence electrode trajectory and intracochlear trauma? Laryngoscope 125 (4), 966–971.